One-Pass List-Mode EM Algorithm for High-Resolution 3-D PET Image Reconstruction Into Large Arrays

Andrew J. Reader, Stijn Ally, Filippos Bakatselos, Roido Manavaki, Richard J. Walledge, Alan P. Jeavons, Peter J. Julyan, Sha Zhao, David L. Hastings, and Jamal Zweit

***Abstract*—High-resolution three-dimensional (3-D) positron emission tomography (PET) scanners with high count rate performance, such as the quad-high density avalanche chamber (HIDAC), place new demands on image reconstruction algorithms due to the large quantities of high-precision list-mode data which are produced. Therefore, a reconstruction algorithm is required which can, in a practical time frame, reconstruct into very large image arrays (submillimeter voxels, which range over a large field of view) whilst preferably retaining the precision of the data. This work presents an algorithm which meets these demands: one-pass list-mode expectation maximization (OPL-EM) algorithm. The algorithm operates directly on list-mode data, passes through the data once only, accounts for finite resolution effects in the system model, and can also include regularization. The algorithm performs multiple image updates during its single pass through the list-mode data, corresponding to the number of subsets that the data have been split into. The algorithm has been assessed using list-mode data from a quad-HIDAC and is compared to the analytic reconstruction method 3-D reprojection (RP) with 3-D filtered backprojection.**

***Index Terms*—Iterative image reconstruction, list mode, positron emission tomography (PET).**

I. Introduction

SMALL animal imaging, which opens new possibilities for biomedical research (e.g., [1]), has called for higher resolution positron emission tomography (PET) scanners combined with high sensitivity. Typically, these systems (such as the quad-high density avalanche chamber (HIDAC) [2] or microPET [3]) produce vast quantities of high-precision list-mode data, thus placing new demands on image reconstruction algorithms. Conventional projection-data based reconstruction techniques can become computationally burdensome for large image arrays (such as $256 \times 256 \times 512$), especially if the precision of the acquired list-mode data is not to be compromised. (Projection-data based reconstruction nearly always involves some loss in the originally acquired list-mode data precision, in order to have practical and manageable four-dimensional (4-D) projection data). Reconstruction directly from list-mode data obviates this information loss in the raw data and is becoming a popular technique in emission tomography [4]–[10]. However, depending on the number of events, iterative reconstruction direct from list-mode data can be costly, and so this work focuses on an algorithm based on just *one pass* through the data, with multiple image updates.

Manuscript received November 23, 2001; revised February 27, 2002.

A. J. Reader, R. Manavaki, and R. J. Walledge are with the Department of Instrumentation and Analytical Science (DIAS) at the University of Manchester Institute of Science and Technology (UMIST), Manchester, M60 1QD, U.K. (e-mail: A.J.Reader@umist.ac.uk).

S. Ally and F. Bakatselos are with Department of Instrumentation and Analytical Science (DIAS) at the University of Manchester Institute of Science and Technology (UMIST), Manchester, M60 1QD, U.K.

A. P. Jeavons is with Oxford Positron Systems, Weston Business Park, Oxford OX6 8SY, U.K. (e-mail: alan@oxpos.co.uk).

P. J. Julyan, S. Zhao, and D. L. Hastings are with the Paterson Institute of Cancer Research and Christie Hospital NHS Trust, Manchester, U.K. (e-mail: Peter.Julyan@physics.cr.man.ac.uk; szhao@picr.man.ac.uk; David.Hastings@physics.cr.man.ac.uk).

J. Zweit is with the Department of Instrumentation and Analytical Science (DIAS) at the University of Manchester Institute of Science and Technology (UMIST), Manchester, M60 1QD, U.K., and also with the Paterson Institute of Cancer Research and Christie Hospital NHS Trust, Withington, Manchester M20 4BX, U.K. (e-mail: jzweit@picr.man.ac.uk).

Publisher Item Identifier S 0018-9499(02)06188-9.

II. Theory

The proposed one-pass list-mode expectation maximization (OPL-EM) algorithm is developed from the standard projection-data based maximum likelihood-expectation maximization (ML-EM) algorithm [11].

A. Projection-Data Based ML-EM

The EM algorithm for ML estimation is given by

$$n_j^{k+1} = \frac{n_j^k}{\sum_{i=1}^{I} a_{ij}} \sum_{i=1}^{I} a_{ij} \frac{m_i}{q_i^k} \text{ with}$$

$$q_i^k = \sum_{j=1}^{J} a_{ij} n_j^k \tag{1}$$

where q_i^k is the expected count in line of response (LOR) i if the intensity was n_j^k (at the kth iteration), a_{ij} is the probability of an emission from voxel j being detected along LOR i, m_i is the number of events collected along LOR i, and I is the number of all possible system LORs. J is the number of voxels in the image.

B. List-Mode ML-EM

List-mode ML-EM is then given by [5], [6]

$$n_j^{k+1} = \frac{n_j^k}{\sum_{i=1}^{I} a_{ij}} \sum_{i=1}^{M} a_{ij} \frac{1}{q_i^k} \tag{2}$$

where the measured list-mode data (simply a list of M line definitions) are now implicitly 1 for each acquired LOR. Equation (2) is a slow algorithm, requiring a complete pass through the list-mode data for each image update.

C. OPL-EM Algorithm

Significant acceleration can be achieved through use of subsets [6] and, in particular, by only passing through the list-mode data *once*, as proposed here. This one-pass algorithm generates a sequence of image estimates n_j^k, where $k(=1,\ldots,K)$ indicates both the iteration number as well as the kth subset of the list-mode data which was used to update the image from n_j^{k-1} to n_j^k. The final image n_j^K is taken as the reconstruction. Thus, the one-pass algorithm is given by

$$n_j^{k+1} = \frac{n_j^k}{\sum_{i=1}^{I} a_{ij}} \sum_{i \in T^k} a_{ij} \frac{1}{q_i^k}, \quad \text{for } k = 1,\ldots,K \tag{3}$$

where the crucial difference is that the summation is now only over those list-mode events i which are present in the kth subset T^k, which is a time subset of the list-mode data. It is of course important to note that convergence to the ML estimate is no longer guaranteed, but in practice this objective is never sought due to its noisy characteristics.

D. Spatially Extensive System Modeling

Of first importance to any implementation of an iterative reconstruction algorithm is the system model (given by the matrix of probabilities $A = (a_{ij})_{I \times J}$). Conventionally, for list-mode reconstruction, a simple model is often used to make the technique feasible, such as calculating the intersection length of LOR i with voxel j to represent the probability a_{ij} (e.g., this can be achieved with the Siddon algorithm [12]). This work proposes a new approach to system modeling for iterative list-mode reconstruction: decomposition of the matrix A into the product of three matrices (which is similar to an approach for use with projection data [13]). The method proposed here permits more flexible and spatially extensive system modeling (without a large computational burden if shift-invariant effects are considered). The only assumption is that the system matrix can be rewritten as

$$A = WXH. \tag{4}$$

The matrix $H = (h_{ij})_{J \times J}$ accounts for finite resolution effects (such as positron range, photon acollinearity, and intrinsic detector resolution) and possibly can be used to model image-wide effects such as scatter and random events. For a given voxel j (in an image to be operated on by H), the matrix H collects counts from a neighborhood around the voxel and places the result in voxel j in an output image. When the next matrix $X = (x_{ij})_{I \times J}$ is applied to this output image (x_{ij} is simply the intersection length of LOR i with voxel j, implemented here by the Siddon forward projection method [12]), the forward projection along the LOR actually includes counts from the local vicinity to the LOR, and not just counts which were exactly on the LOR. Finally, the diagonal matrix $W = (w_{ii})_{I \times I}$ allows a weight be assigned to each LOR, to account for geometric sensitivity variations, such as detector rotation. So the expected count q_i^k in each LOR i, if the image estimate is n_j^k, is found by

$$q_i^k = w_{ii} \sum_{j=1}^{J} x_{ij} \sum_{b=1}^{J} h_{jb} n_b^k. \tag{5}$$

Equation (5) shows that the image estimate n_j^k is first preprocessed according to the blurring kernels $\{h_{ij}\}$ contained in H (which can be shift-invariant for a fast and straightforward convolution-based implementation). This modified image is then forward projected through using X (for a fast and straightforward implementation, Siddon's method can be used). The prior use of H incorporates more data into the calculation of the expected data q_i^k, improving the statistical quality of the correction factor $1/q_i^k$.

So, by substituting for the new expression for A into (3), the OPL-EM algorithm becomes

$$n_j^{k+1} = \frac{n_j^k}{\sum_{b=1}^{J} h_{bj} \sum_{i=1}^{I} w_{ii} x_{ib}} \sum_{b=1}^{J} h_{bj} \sum_{i \in T^k} x_{ib} \times \frac{1}{\sum_{p=1}^{J} x_{ip} \sum_{v=1}^{J} h_{pv} n_v^k}. \tag{6}$$

E. Regularization

Even though the algorithm is restrained to one pass through the list-mode data and incorporates a more accurate system model, regularization could still (in general) be required, to counteract the ill-conditioning of the inverse problem. (However, high-quality results are obtained using the above algorithm (6), without the need for regularization). This work uses a regularization approach similar in principle to the methods by Snyder *et al.* [14]. Rather than first reconstruct and then post-filter, the method here incorporates the chosen level of smoothing directly into the reconstruction process. The level of smoothing is determined by a Gaussian function of a chosen full-width at half-maximum (FWHM). To describe the method used, first (6) is rewritten in terms of J-dimensional vectors

$$\mathbf{n^{k+1}} = \mathbf{n^k} \times \mathbf{s} \times \mathbf{c^k} \tag{7}$$

where $\times$ denotes an element-by-element multiplication between two J-dimensional vectors. $\mathbf{n^{k+1}}$ and $\mathbf{n^k}$ contain the image values of the new and old image estimates, respectively, and $\mathbf{s}$ contains the sensitivity correction factors (mainly due to scanner geometry). $\mathbf{c^k}$ contains the multiplicative image correction values, given by

$$\mathbf{c^k} = H^T \left[\sum_{i \in T^k} \mathbf{BP_i} \left(\frac{1}{\mathrm{FP}_i(H\mathbf{n^k})} \right) \right] \tag{8}$$

where the matrix H (as defined above) is multiplied by a J-dimensional vector to give a new J-dimensional vector, FP_i is an operator which forward projects along LOR i through a 3-D image (represented as a J-D vector) to give a scalar value, and $\mathbf{BP_i}$ is an operator which backprojects a scalar value along an LOR i into a 3-D image. Note that H and H^T (its transpose) need only be applied once for a given iteration k, and not for each and every LOR i, which is the key point to the technique.

The regularization method used here constrains the update formula (7) by smoothing the correction image [given by (8)] with a kernel κ, so that (7) becomes

$$\mathbf{n^{k+1}} = \mathbf{n^k} \times \mathbf{s} \times \left[\mathbf{c^k} \otimes \kappa\right] \tag{9}$$

where $\otimes$ denotes convolution of the 3-D image (stored as a J-D vector) with a kernel, to give a new vector. This constraint is incorporated within the reconstruction process, as opposed to applying the convolution operation after reconstruction as a last step remedial action for noise. When this type of regularization is applied, the OPL-EM algorithm becomes

$$\mathbf{n^{k+1}} = \mathbf{n^k} \times \mathbf{s} \times \left\{ \left(H^T \left[\sum_{i \in T^k} \mathbf{BP_i} \left(\frac{1}{\mathrm{FP}_i\left(H\mathbf{n^k}\right)} \right) \right] \right) \otimes \kappa \right\}. \tag{10}$$

Finally, for fast implementation, the spatially extensive (blurring) component H of the system matrix can be represented as a set of shift-invariant kernels ρ (resolution blurring is thus assumed invariant across the image). So, when using convolution for resolution modeling, and when including regularization, OPL-EM is given by

$$\mathbf{n^{k+1}} = \mathbf{n^k} \times \mathbf{s} \times \left\{ \left(\left[\sum_{i \in T^k} \mathbf{BP_i} \left(\frac{1}{\mathrm{FP}_i\left(\mathbf{n^k} \otimes \rho\right)} \right) \right] \otimes \rho \right) \otimes \kappa \right\}. \tag{11}$$

OPL-EM therefore has three parameters: the choice of resolution kernel ρ, the choice of smoothing kernel κ, and the number (K) of subsets to use (each subset labeled T^k, $k = 1, \ldots, K$, where K is also the number of image updates to perform).

III. Evaluation

A. Composite Phantom: Cylinders and Line Sources

To assess resolution and noise, a cylindrical phantom (30-mm-diameter, 50-mm-long) containing four smaller cylindrical inserts with total activities of 2.13, 0.94, 0.39, and 0.29 MBq (^{18}F) with a background containing 0.12 MBq was scanned for 1 h with the quad-HIDAC tomograph. One hundred six million events were acquired. Also, a 0.5-mm-diameter ^{22}Na line source ($<$1 MBq), of length 100 mm, was scanned in three different positions of the field of view (FOV): (on axis, 30 mm off axis, and transverse to the axis). In each case, approximately 10 million events were acquired in 20, 25, and 30 min, respectively. These three line-source data sets were merged with part of the list-mode data from the cylindrical phantom, in the ratio 1:1:1:2, to result in a synthesized data set consisting of 50 million events. This data set allowed noise and resolution properties of the reconstruction algorithm to be assessed, but it should be noted that the level of randoms in the synthesized data set is lower than what would be obtained had the lines and cylinders been acquired in a single scan. The data were reconstructed with OPL-EM and the analytic 3-D reprojection (RP) method [15], into 256^3 image arrays of 0.3-mm voxels, giving an FOV of 76.8 mm in diameter and 76.8 mm in axial extent. For OPL-EM, five choices of ρ were tested (Gaussians with FWHMs of 0, 0.5, 1, 1.5, and 2 mm), and three choices of smoothing kernel κ were tested (Gaussians with FWHMs of 0, 0.6, and 0.9 mm). Thus, a total of 15 OPL-EM reconstructions were performed. For the 3-D RP reconstructions, three choices of smoothing were used: no smoothing, a Hanning window with cutoff at 100% of the Nyquist frequency, and also with a cutoff at 80%.

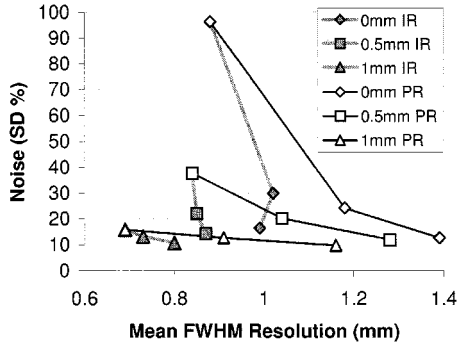

Fig. 1. Results from reconstructions of the composite (cylinders + lines) phantom. The comparison is between regularization incorporated inside the reconstruction process (IR) and "regularization" applied as a post-reconstruction convolution (PR), for different resolution kernels ($\rho = 0$ mm, $\rho = 0.5$ mm and $\rho = 1.0$ mm FWHM Gaussian). The mean FWHM resolution of the reconstructed lines is plotted versus the noise in the hottest cylindrical insert. For a given noise level in the uniform cylindrical insert, there is a significant improvement in resolution when regularization is implicitly incorporated into the reconstruction algorithm (IR). Results are shown for different regularization kernels ($\kappa = 0.0$, 0.6, and 0.9 mm FWHM Gaussians). Fifty updates ($K = 50$) were used for these reconstructions of 50 million events into 256^3 arrays (0.3-mm voxels). Note that the substantial level of noise reduction achieved by using resolution modeling significantly reduces the need for any incorporation of regularization.

The noise in each reconstruction was evaluated according to the standard deviation of the voxel values about the mean value in a subregion of each of the four cylindrical inserts. The resolution was simply taken as the mean FWHM of every available cross section of the three line sources—which yielded numerous measures of radial, tangential, and axial resolution.

To assess the regularization technique, it was compared with a post-reconstruction convolution operation (using Gaussians with FWHMs of 0, 0.6, and 0.9 mm).

No corrections for scatter, attenuation, randoms, detector efficiency, dead time, or radioisotope decay were included in these reconstructions.

B. Rat Scans

As a means of qualitative assessment, OPL-EM was used to reconstruct an ^{18}F rat bone scan and an ^{18}FDG rat scan.

IV. Results and Analysis

A. Cylindrical Phantom and Line Sources

First, Fig. 1 shows that if regularization is to be included, it is advantageous to incorporate the smoothness constraint inside the reconstruction algorithm. Smoothing the correction image according to κ achieves very similar levels of noise reduction compared to post-reconstruction smoothing, but quite crucially maintains a significantly better level of resolution in the resulting images.

Fig. 2 plots resolution versus noise for the composite (cylinders and lines) phantom. It is clear that the OPL-EM algorithm is superior to 3-D RP. For this case, the optimum choice of ρ to model the resolution of the measurement process (i.e.,

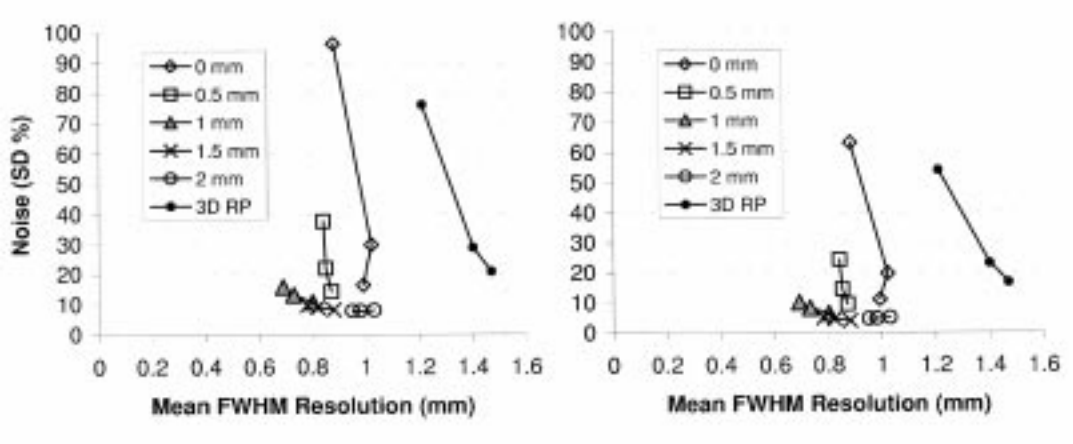

Fig. 2. Results from reconstructions of the composite (cylinders + lines) phantom. Mean resolution for the three line sources versus noise in the two hottest cylindrical inserts (hence two graphs, the hottest on the left, with the second hottest on the right) is shown. The OPL-EM algorithm is shown for five different choices of the resolution modeling kernel ρ (Gaussian FWHM of 0 mm, 0.5 mm, 1 mm, 1.5 mm, and 2 mm) and for three different choices of the regularization kernel κ (Gaussian functions of 0 mm, 0.6 mm, and 0.9 mm FWHM). The 3-D RP algorithm is shown for three choices of smoothing (no smoothing, a Hanning window with a cutoff at 100% of the Nyquist frequency, and with a cutoff at 80% of the Nyquist frequency).

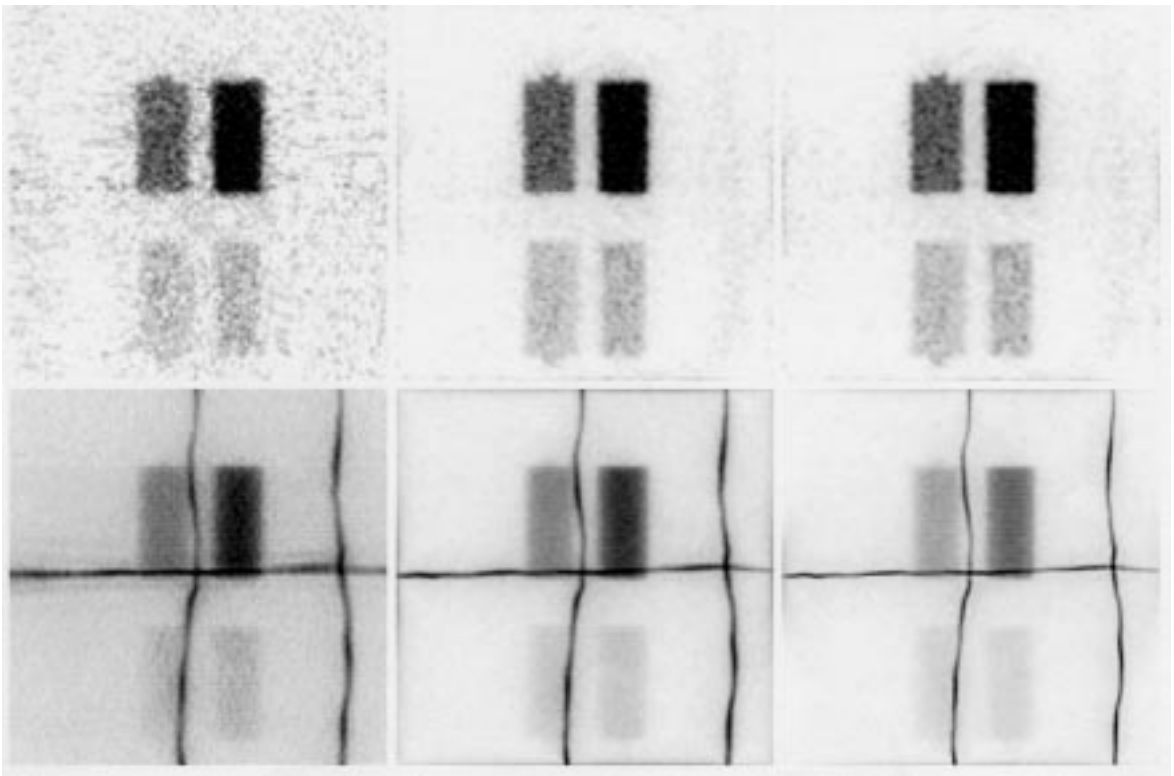

Fig. 3. Reconstructions of the composite (cylinders + lines) phantom. Top row: single coronal slice through the 3-D reconstruction of the cylindrical phantom, for 3-D RP (left, Hanning window with cutoff at 80% Nyquist), OPL-EM (middle, without resolution modeling: $\rho = 0$ mm, but with regularization $\kappa = 0.9$ mm) and for OPL-EM with resolution modeling (right, $\rho = 1.0$ mm, $\kappa = 0$ mm). Bottom row: summed coronal slices. These particular images were selected due to their very similar noise measures within the cylindrical inserts, and the difference in resolution between the techniques for this given noise level is very apparent, clearly improving from left to right. This improvement can be understood as: (left) 3-D RP: projection-data analytic reconstruction, (middle) OPL-EM without resolution modeling: iterative list-mode reconstruction, (right) OPL-EM with resolution modeling: iterative list-mode reconstruction. [0.3-mm voxels, 3-D image array of size $256 \times 256 \times 256$, covering 76.8 mm in each dimension].

positron range, finite detector resolution etc.) is a 1-mm FWHM Gaussian. Note how important accurate system modeling is: the figure clearly shows that, by using more accurate system modeling (i.e., accounting for finite resolution), not only is resolution enhanced—as would be expected when trying to "recover" resolution—but, quite significantly, there is also substantial image noise reduction.

Fig. 3 shows example reconstructions of the composite phantom for similar noise levels, showing the variation in resolution between techniques.

Fig. 4 looks at the issue of convergence for the OPL-EM algorithm. The single pass through the data, inherent to OPL-EM, yields an image estimate which actually lies on the noise-resolution tradeoff curve obtained when different regularization pa-

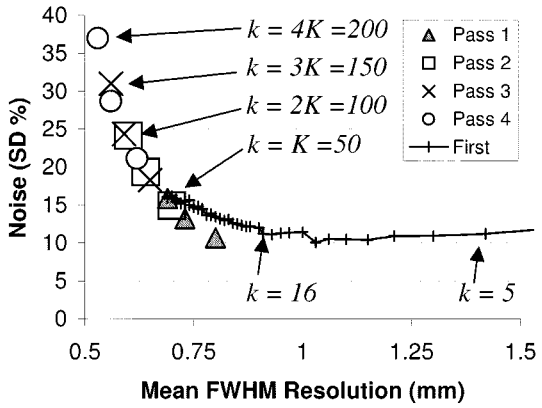

Fig. 4. Noise and resolution evaluated for: i) each image estimate created during the single pass through the list-mode data (i.e., $K = 50$ images, $k = 1, \ldots, 50$, were analyzed) and ii) for four complete passes through the list-mode data (3 points are given for each case, according to the choice of regularization kernel κ: 0 mm, 0.6 mm, and 0.9 mm FWHM Gaussian). The first pass through the data ($k = 1, \ldots, 50$) gives the most substantial improvements in noise and resolution, with further passes through the data just modifying the position along the noise-resolution tradeoff curve in a manner virtually identical to modifying the choice of regularization kernel. So a single pass through the data with $\kappa = 0$ mm mimics the result of two passes through the data with $\kappa = 0.9$ mm—showing that iterations merely control the choice of smoothness for the reconstruction of this particular cylinder + lines phantom (which has both high-resolution components and uniform regions).

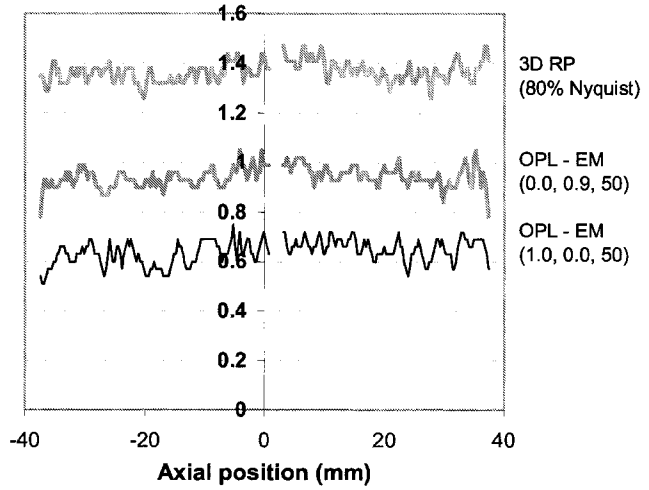

Fig. 5. Plot of axial position in an FOV (x axis) versus radial resolution (FWHM in mm) for three different reconstructions of the composite phantom at a similar noise level. The three images chosen correspond to the three images shown in Fig. 3. It is very evident that OPL-EM with regularization is better than 3-D RP, and that OPL-EM using resolution modeling is better still. The three numbers in brackets for OPL-EM correspond to the FWHM of ρ, the FWHM of κ (both in mm), and the number of subsets K, respectively.

rameters are chosen for multiple passes through the list-mode data. Using just one pass through the data results in an image which is at the lower noise end of this tradeoff curve. In fact, the graph shows that one pass through the data without regularization gives a result equivalent to *two* passes through the data *with* regularization. (Thus, an inter-play between the number of passes through the data and the chosen regularization is apparent). Of course, this result is unique to the phantom considered and the number of events used, but the phantom (which contains both high-resolution components as well as uniform regions) provides a representative activity distribution for real imaging situations.

TABLE I
RECONSTRUCTION TIMES

Events and Matrix Size	3D RP (3D FBP)	OPL-EM	OPL-EM (factored)
54 million (256×256×256)	4h 9m	7h 8m	3h 58m
145 million (256×256×512)	5h 11m	23h 45m	12h 30m

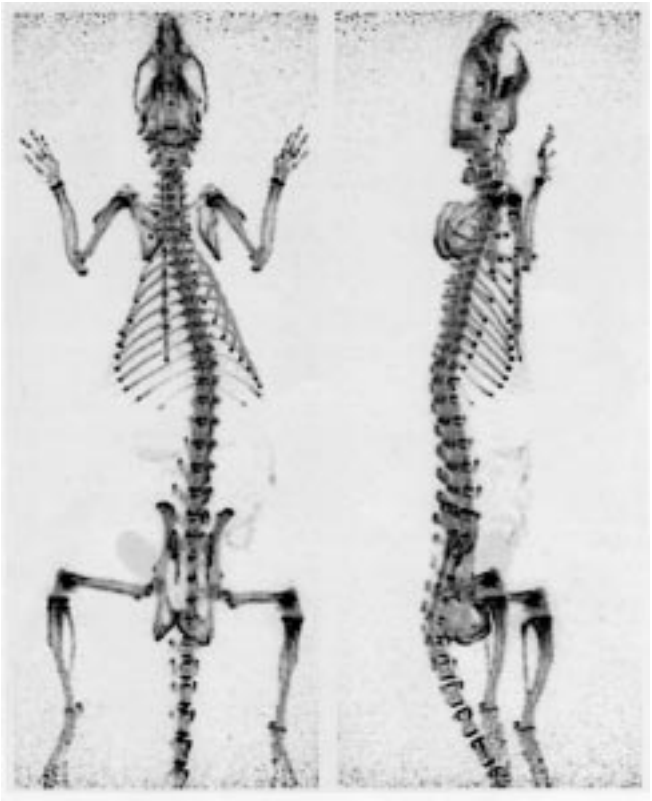

Fig. 6. Maximum intensity coronal projection (left) and maximum intensity sagittal projection (right) of the 3-D OPL-EM reconstruction of the ^{18}F rat bone scan. One hundred forty-five million list-mode events were reconstructed into a $250 \times 250 \times 620$ array (0.45-mm voxel side). Storage space for the image was ~150 Mbytes. Resolution was modeled with a shift-invariant Gaussian kernel ρ with an FWHM of 1.35 mm. No regularization was used ($\kappa = 0$ mm Gaussian). $K = 75$ subsets (and so also 75 updates) were chosen. A nonlinear gray scale has been used to reveal the detail. [17 MBq of ^{18}F, 500 g rat, 30-min acquisition time for 145×10^6 events].

Fig. 5 compares resolution for a given level of image noise. Again, the improvement of using iterative list-mode reconstruction can be seen, particularly in the case where resolution is modeled. Table I compares reconstruction times. Reconstruction time [hours (h) and minutes (m)] for OPL-EM and 3-D RP is given in Table I. 3-D RP time includes binning of the list-mode data into a 4-D projection matrix. OPL-EM used $\rho = 1.0$ mm, $\kappa = 0$ mm, and $K = 50$ for the 54 million event data set, and $\rho = 1.35$ mm, $\kappa = 0$ mm, and $K = 75$ for the 145 million event data set. The factored version of OPL-EM used simple 1D convolutions instead of truly 3-D convolution operations. Times given are for a 667-MHz Alpha XP1000 workstation.

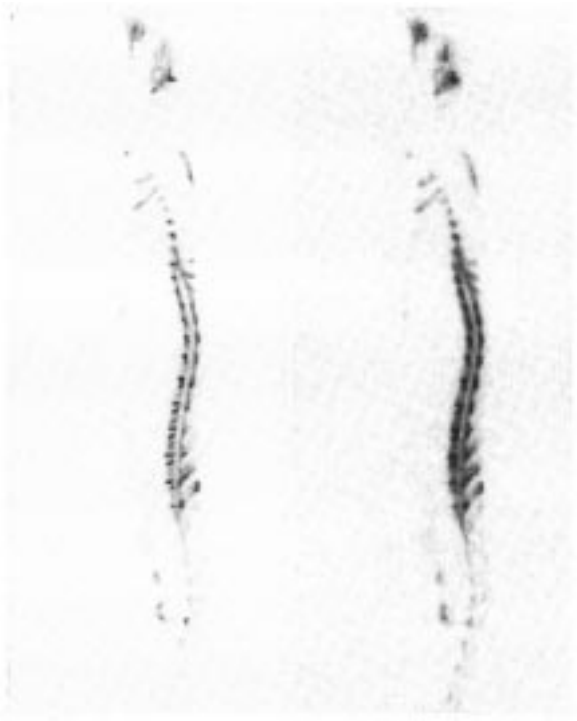

Fig. 7. Sagittal slice through the 3-D reconstruction of the ^{18}F rat bone scan, for OPL-EM (left) and 3-D RP (right). The OPL-EM reconstruction is the same as that in Fig. 6, but the image has been truncated to match the size of the 3-D RP reconstruction ($256 \times 256 \times 512$). For the 3-D RP reconstruction, the list-mode data were binned into a $256 \times 512 \times 64 \times 17$ projection array (0.45 mm bin side, 2.8° azimuthal sampling, 5.9° copolar sampling) which required 570 Mb storage. [For improved sampling of the projection data, storage becomes a very significant issue].

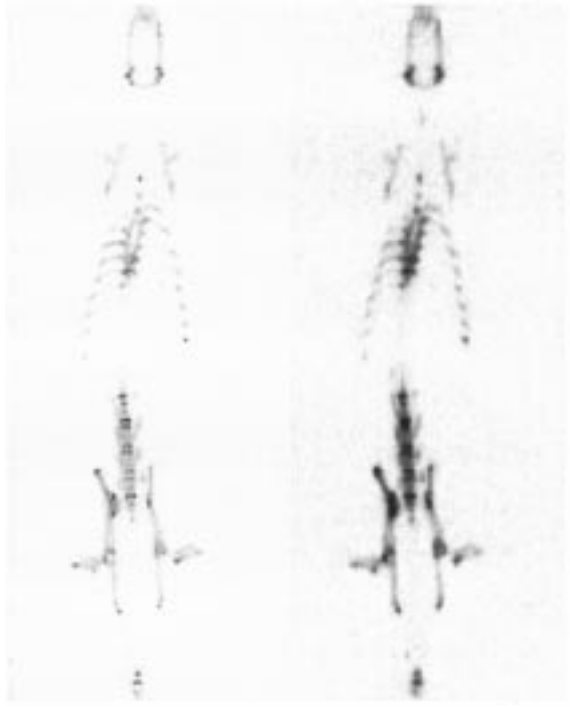

Fig. 8. Coronal slices through the 3-D reconstruction of the ^{18}F rat bone scan, for OPL-EM (left) and 3-D RP (right). The OPL-EM and 3-D RP reconstructions are the same as those in Fig. 7.

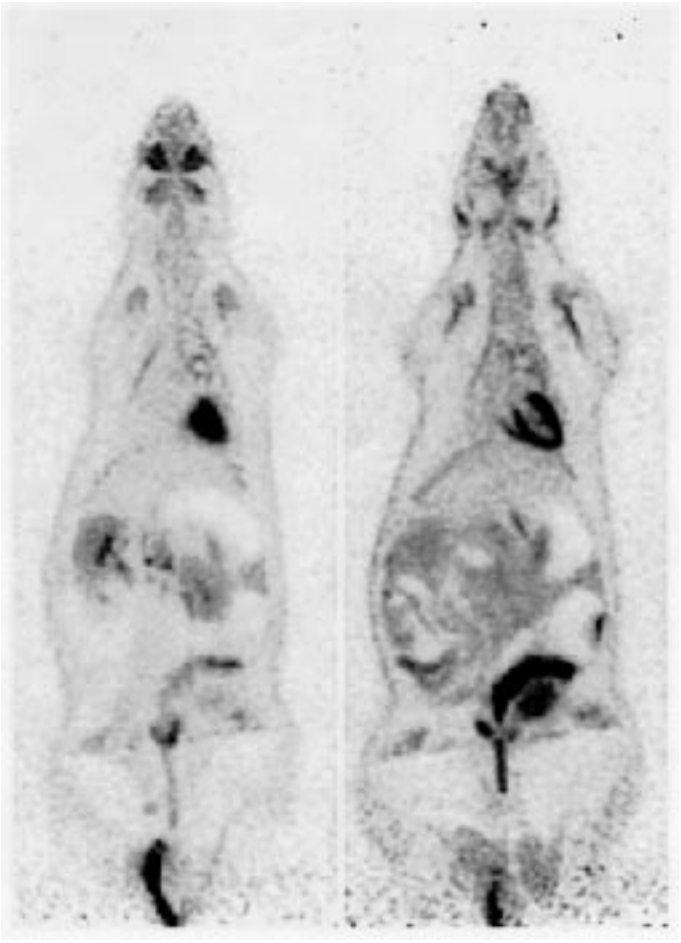

Fig. 9. Coronal slices through the 3-D reconstruction of the ^{18}FDG rat scan for OPL-EM. 214 million list-mode events were reconstructed into a $200 \times 200 \times 560$ array (0.5 mm voxel side). Resolution was modeled with a 1.5 mm FWHM Gaussian (ρ) No regularization was used ($\kappa = 0$ mm). $K = 75$ subsets (and so also 75 updates) were chosen. [8.74 MBq of ^{18}FDG, 430 g rat, 90-min acquisition time for 214×10^6 events].

B. Rat Scans

Figs. 6–9 compare OPL-EM and 3-D RP reconstructions of the rat bone and FDG (OPL-EM only) scans.

V. Conclusion

The new list-mode EM algorithm, OPL-EM, based on one pass through the list-mode data, is a practical and competitive method for reconstruction directly from list-mode data. The OPL-EM algorithm has four key points to its success: 1) it uses list-mode data directly to preserve full sampling precision of the data; 2) it only uses one-pass through the list-mode data to ensure practicality of the algorithm; 3) it uses spatially extensive system modeling, to account for finite resolution effects; and 4) it allows incorporation of regularization directly as part of the reconstruction process.

Acknowledgment

The authors gratefully acknowledge Dr. Missimer, Dr. Honer, Dr. H. Ametamey, and Prof. Schubiger (Paul Scherrer Institute) for supplying the raw list-mode data for the rat scans.

REFERENCES

[1] A. J. Reader and J. Zweit, "Developments in whole body molecular imaging of live subjects," *Trends in Pharmacological Sci.*, vol. 22, pp. 604–607, 2001.

[2] A. P. Jeavons, R. A. Chandler, and C. A. R. Dettmar, "A 3D HIDAC-PET camera with sub-millimeter resolution for imaging small animals," *IEEE Trans. Nucl. Sci.*, vol. 46, pp. 468–473, 1999.

[3] Y. C. Tai, A. Chatziioannou, S. Siegel, J. Young, D. Newport, R. N. Goble, R. E. Nutt, and S. R. Cherry, "Performance evaluation of the microPET p4: A PET system dedicated to animal imaging," *Phys. Med. Biol.*, vol. 46, pp. 1845–1862, 2001.

[4] H. H. Barrett, T. White, and L. C. Parra, "List-mode likelihood," *J. Opt. Soc. Amer. A*, vol. 14, pp. 2914–2923, 1997.

[5] L. Parra and H. H. Barrett, "List-mode likelihood: EM algorithm and image quality estimation demonstrated on 2-D PET," *IEEE Trans. Med. Imaging*, vol. 17, pp. 228–235, 1998.

[6] A. J. Reader, K. Erlandsson, M. A. Flower, and R. J. Ott, "Fast accurate iterative reconstruction for low-statistics positron volume imaging," *Phys. Med. Biol.*, vol. 43, pp. 835–846, 1998.

[7] J. A. Patton, E. Shai, M. Wilk, G. Harden, and M. P. Sandler, "Evaluation of COSEM, a new iterative reconstruction algorithm for coincidence imaging," *J. Nucl. Med.*, vol. 40, no. 5, pp. 1295–1295, 1999.

[8] R. Huesman, G. Klein, W. Moses, J. Qi, B. Reutter, and P. Virador, "List-mode maximum likelihood reconstruction applied to positron emission mammography (PEM) with irregular sampling," *IEEE Trans. Med. Imaging*, vol. 19, pp. 532–537, 2000.

[9] C. Byrne, "Likelihood maximization for list-mode emission tomographic image reconstruction," *IEEE Trans. Med. Imaging*, vol. 20, pp. 1084–1092, 2001.

[10] L. Bouwens, R. Van de Walle, H. Gifford, M. King, I. Lemahieu, and R. A. Dierckx, "LMIRA: List-mode iterative reconstruction algorithm for SPECT," *IEEE Trans. Nucl. Sci.*, vol. 48, pp. 1364–1370, 2001.

[11] L. A. Shepp and Y. Vardi, "Maximum likelihood reconstruction for emission tomography," *IEEE Trans. Med. Imaging*, vol. MI-1, pp. 113–122, 1982.

[12] R. L. Siddon, "Fast calculation of the exact radiological path for a three-dimensional CT array," *Med. Phys.*, vol. 12, pp. 252–255, 1985.

[13] E. U. Mumcuoglu, R. Leahy, S. R. Cherry, and Z. Zhou, "Fast gradient based methods for bayesian reconstruction of transmission and emission PET images," *IEEE Trans. Med. Imaging*, vol. 13, pp. 687–701, 1994.

[14] D. L. Snyder, M. I. Miller, L. J. Thomas, and D. G. Politte, "Noise and edge artifacts in maximum-likelihood reconstructions for emission tomography," *IEEE Trans. Med. Imaging*, vol. 6, pp. 228–238, 1987.

[15] P. E. Kinahan and J. G. Rogers, "Analytic three-dimensional image reconstruction using all detected events," *IEEE Trans. Nucl. Sci.*, vol. 36, pp. 964–968, 1989.